1 August 2002

Optics Communications 209 (2002) 45–54

OPTICS COMMUNICATIONS

www.elsevier.com/locate/optcom

Polarization beam-splitters and optical switches based on space-variant computer-generated subwavelength quasi-periodic structures

Erez Hasman*, Ze'ev Bomzon, Avi Niv, Gabriel Biener, Vladimir Kleiner

Optical Engineering Laboratory, Faculty of Mechanical Engineering, Technion-Israel Institute of Technology, Haifa 32000, Israel

Received 12 April 2002; accepted 13 May 2002

Abstract

Polarization beam-splitters and optical switches based on subwavelength quasi-periodic structures are presented. By locally controlling the orientation and period of the subwavelength grooves, birefringent elements for which the optical axes vary periodically, are realized. We present a theoretical discussion of these elements, as well as a detailed description of the design and realization procedures. We show experimental results for infra-red radiation at a wavelength of 10.6 μm. © 2002 Elsevier Science B.V. All rights reserved.

PACS: 42.25 Bs; 42.25.Ja; 42.79.Dj

Keywords: Wave propagation; Polarization; Gratings

1. Introduction

Polarizing beam-splitters are essential components in polarization-based systems such as ellipsometers, magneto-optic data storage and polarization-based light modulators. Often these applications require that the elements provide high extinction ratios over a wide angular bandwidth while maintaining compact and efficient packaging. Conventional polarizing beam-splitters, employing either natural crystal birefringence or polarization-sensitive multilayer structures are usually, either cumbersome or sensitive to angular change, and therefore do not fully meet these requirements.

Contemporary research has begun to address the use of polarization diffraction gratings as beam-splitters and optical switches. Unlike scalar diffraction gratings that are based on periodic modification of phase and amplitude, polarization diffraction gratings introduce a periodic spatial change of the state of polarization leading to polarization-dependent diffraction. Furthermore, the polarization of the diffracted orders is generally different from that of the incident beam. Such a device was demonstrated by Davis et al. [1] who used liquid crystals to create a waveplate with space-varying retardation. Alternatively, Gori [2]

* Corresponding author. Fax: +972-4-832-4533.
E-mail address: mehasman@tx.technion.ac.il (E. Hasman).

0030-4018/02/$ - see front matter
PII: S0030-4018(02)01598-5

suggested a grating consisting of a polarizer with a spatially rotating transmission axis and Tervo and Turunen [3] suggested that beam-splitters consisting of spatially rotating wave-plates could be realized using subwavelength gratings. More recently a polarization diffraction grating based on spatially rotating nematic liquid crystals has been demonstrated [4].

In previous papers we demonstrated space-variant polarization-state manipulations using computer-generated subwavelength structures [5–7]. When the period of a subwavelength periodic structure is smaller than the incident wavelength, only the zeroth order is a propagating order, and all other orders are evanescent. The subwavelength periodic structure behaves as a uniaxial crystal with the optical axes parallel and perpendicular to the subwavelength grooves. Therefore, by fabricating quasi-periodic subwavelength structures, for which the period and orientation of the subwavelength grooves was space-varying, we realized continuously rotating waveplates and polarizers for CO_2 laser radiation at a wavelength of 10.6 μm. Furthermore, we showed that such polarization manipulations necessarily led to phase modification of geometrical origin, which left a clear signature on the propagation of the resulting wave. The phase introduced did not result from optical path differences but solely from local changes in polarization and was infact a manifestation of the geometrical Pancharatnam–Berry phase [8].

In this paper we present an experimental demonstration of polarization diffraction gratings based on space-variant computer-generated subwavelength structures. We present a novel interpretation of these elements and show that the polarization-related diffraction is indeed connected to the space-varying Pancharatnam–Berry phase mentioned above. We present experimental results for infra-red CO_2 laser radiation that include a polarization diffraction grating based on a space-variant continuous metal-stripe subwavelength structure, a continuously rotating dielectric subwavelength structure and a binary waveplate, for which the direction of the subwavelength grooves varies discretely. We also demonstrate a circular symmetric polarization mode switching based on a computer-generated subwavelength structure, thus enabling alternation between intensity distributions of a bright and dark center.

2. Theoretical analysis of the polarization diffraction gratings

Fig. 1 is a schematic representation of the use of a subwavelength structure as a polarization diffraction grating. The local orientation of the subwavelength grooves, $\theta(x)$, varies linearly in the x-direction, to form a polarization diffraction grating comprising a birefringent element with optical axes (which are parallel and perpendicular to the grating grooves) that rotate periodically in the x-direction. The period of the polarization diffraction grating, d, is larger than the incident wavelength, λ, whereas the local subwavelength period of the grooves, $\Lambda(x,y)$, is smaller than the incident wavelength. When a plane-wave with uniform polarization is incident on such a periodic subwavelength structure, the transmitted field will be periodic in both polarization and phase, therefore, we can expect this field to yield discrete diffraction orders in the far-field.

It is convenient to describe subwavelength quasi-periodic structures such as the one depicted in Fig. 1 using Jones calculus. In this representation, a uniform periodic subwavelength structure

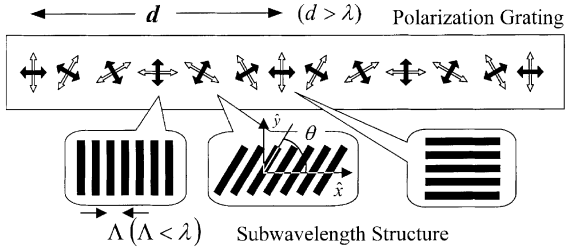

Fig. 1. Illustration of the concept of polarization diffraction gratings fabricated using subwavelength quasi-periodic structures. The orientation of the subwavelength grooves, $\theta(x)$ varies periodically in the x-direction, resulting in an element with effective birefringence, whose optical axes (marked by the dark and light arrows in the picture), rotate periodically. The polarization diffraction grating has period d, which is larger than the incident wavelength, λ, whereas the local subwavelength period is $\Lambda < \lambda$. The local optical axes at each point are oriented parallel and perpendicular to the subwavelength grooves.

the grooves of which are oriented along the y-axis can be described by the Jones matrix

$$\mathbf{J} = \begin{pmatrix} t_x & 0 \\ 0 & t_y e^{i\phi} \end{pmatrix}, \tag{1}$$

where t_x, t_y are the real amplitude transmission coefficients for light polarized perpendicular and parallel to the optical axes and ϕ is the retardation of the grating. If the orientation of the subwavelength grooves is space-varying, i.e., different at each location, then the subwavelength structure can be described by the space-dependent matrix

$$\mathbf{T}_C(x) = \mathbf{M}(\theta(x))\mathbf{J}\mathbf{M}^{-1}(\theta(x)), \tag{2}$$

where $\theta(x)$ is the local orientation of the optical axis and

$$\mathbf{M}(\theta) = \begin{pmatrix} \cos\theta & -\sin\theta \\ \sin\theta & \cos\theta \end{pmatrix}$$

is a two-dimensional rotation matrix.

For convenience we adopt the Dirac bra-ket notation, and convert $\mathbf{T}_C(x)$ to the helicity base in which

$$|\mathbf{R}\rangle = \begin{pmatrix} 1 \\ 0 \end{pmatrix} \quad \text{and} \quad |\mathbf{L}\rangle = \begin{pmatrix} 0 \\ 1 \end{pmatrix}$$

are the two-dimensional unit vectors for right-hand and left-hand circularly polarized light. In this base, the space-variant polarization operator is described by the matrix, $\mathbf{T}(x) = \mathbf{U}\mathbf{T}_C\mathbf{U}^{-1}$, where

$$\mathbf{U} = \frac{1}{\sqrt{2}} \begin{pmatrix} 1 & 1 \\ -i & i \end{pmatrix}$$

is a unitary conversion matrix. Explicit calculation of $\mathbf{T}(x)$ yields

$$\mathbf{T}(x) = \frac{1}{2}\left(t_x + t_y e^{i\phi}\right)\begin{pmatrix} 1 & 0 \\ 0 & 1 \end{pmatrix} + \frac{1}{2}\left(t_x - t_y e^{i\phi}\right) \times \begin{pmatrix} 0 & \exp[i2\theta(x)] \\ \exp[-i2\theta(x)] & 0 \end{pmatrix}. \tag{3}$$

Thus for an incident plane-wave with arbitrary polarization $|\mathbf{E}_{in}\rangle$ we find that the resulting field is

$$|\mathbf{E}_{out}\rangle = \sqrt{\eta_E}|\mathbf{E}_{in}\rangle + \sqrt{\eta_R}e^{i2\theta(x,y)}|\mathbf{R}\rangle + \sqrt{\eta_L}e^{-i2\theta(x,y)}|\mathbf{L}\rangle, \tag{4}$$

where

$$\eta_E = |\tfrac{1}{2}(t_x + t_y e^{i\phi})|^2,$$
$$\eta_R = |\tfrac{1}{2}(t_x - t_y e^{i\phi})\langle \mathbf{E}_{in}|\mathbf{L}\rangle|^2,$$
$$\eta_L = |\tfrac{1}{2}(t_x - t_y e^{i\phi})\langle \mathbf{E}_{in}|\mathbf{R}\rangle|^2,$$

are the polarization order coupling efficiencies and $\langle\alpha|\beta\rangle$ denotes inner product.

Fig. 2 is a graphic representation of the results of Eq. (4). It shows that $|\mathbf{E}_{out}\rangle$ comprises three polarization orders: the $|\mathbf{E}_{in}\rangle$ polarization order (EPO), the $|\mathbf{R}\rangle$ polarization order (RPO) and the $|\mathbf{L}\rangle$ polarization order (LPO). The EPO maintains the polarization and phase of the incident beam, whereas the phase of the RPO is equal to $2\theta(x)$, and the phase of the LPO is equal to $-2\theta(x)$. We note that the phase modification of the $|\mathbf{R}\rangle$ and the $|\mathbf{L}\rangle$ polarization orders results solely from local changes in polarization and is therefore geometrical in nature. We therefore denote this phase as the diffractive geometrical phase (DGP) [9].

The DGP for the $|\mathbf{R}\rangle$ polarization order is opposite in sign to that of the $|\mathbf{L}\rangle$ polarization order, and if $\theta(x)$ is periodic, the functions $e^{i2\theta(x)}$ and $e^{-i2\theta(x)}$ that appear in Eq. (4) can be developed into Fourier series. Taking into account the connection between the Fourier series of a function and the

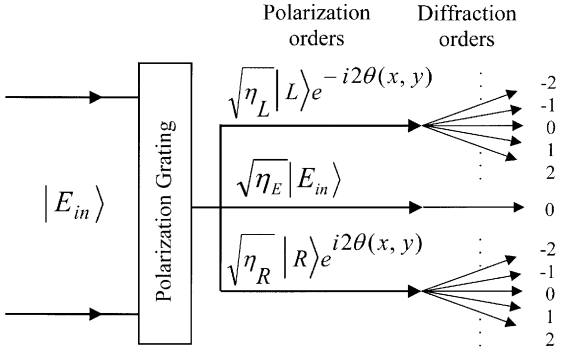

Fig. 2. A diagram describing the operation of polarization diffraction gratings. A beam with polarization $|\mathbf{E}_{in}\rangle$ is incident on the polarization grating. The resulting beam comprises three polarization orders, the EPO, which maintains the original polarization and does not undergo phase modification. The RPO that is $|\mathbf{R}\rangle$ polarized, and whose phase is modified by $2\theta(x)$ and the LPO that is $|\mathbf{L}\rangle$ polarized, and whose phase is modified by $-2\theta(x)$ Since $\theta(x)$ is periodic, the RPO and the LPO undergo diffraction, resulting in the appearance of discrete diffraction orders.

Fourier series of its complex conjugate, this leads to the equation

$$|\mathbf{E}_{\text{out}}\rangle = \sqrt{\eta_0}|\mathbf{E}_{\text{in}}\rangle + \sqrt{\eta_{\text{R}}}\sum_{m=-\infty}^{\infty} a_m e^{i2\pi mx/d}|\mathbf{R}\rangle + \sqrt{\eta_{\text{L}}}\sum_{m=-\infty}^{\infty} a^*_{-m} e^{i2\pi mx/d}|\mathbf{L}\rangle, \quad (5)$$

where

$$a_m = \frac{1}{2\pi}\int e^{i2\theta(x)} e^{i2\pi mx/d}\,dx.$$

Thus we find that the diffraction efficiency into the mth order of the RPO ($\eta^{\text{R}}_m = |a_m|^2$), is equal to the diffraction efficiency into the $-m$th order of the LPO ($\eta^{\text{L}}_{-m} = |a^*_m|^2$), and conclude that the RPO and LPO are diffracted in opposite senses.

Based on Eqs. (4) and (5) we find that there are three degrees of freedom associated with the design of polarization diffraction gratings. The first degree of freedom is the determination of the subwavelength structure parameters, t_x, t_y and ϕ. These parameters determine the amount of energy coupled into the EPO. The second degree of freedom is the grating orientation $\theta(x)$. $\theta(x)$ that determines the DGP, thereby determining the diffraction efficiency into all diffraction orders. The third degree of freedom is the incident polarization $|\mathbf{E}_{\text{in}}\rangle$. It determines the ratio between the energy in the RPO and the energy in the LPO. In the next three sections, we intend to demonstrate how these three degrees of freedom can be utilized for the design and realization of polarization beam-splitters and optical switches using subwavelength quasi-periodic structures.

3. Continuous blazed polarization diffraction gratings

Supposing we wish to design a blazed polarization diffraction grating, i.e., a grating for which all the diffracted energy is in the first-order when the incident beam is $|\mathbf{R}\rangle$ polarized. For $|\mathbf{E}_{\text{in}}\rangle = |\mathbf{R}\rangle$ we find that $\eta_{\text{R}} = 0$. Consequently the transmitted beam only consists of the LPO and the EPO. Since the EPO does not undergo any phase modification, all of its energy is located in the zero-order, and the only order that contributes energy to the first-order is the LPO. In order to ensure that all the energy of the LPO will be diffracted into the first-order, it is required that the DGP for the LPO be equal to $2\pi x/d|_{\text{mod}2\pi}$. Consequently, we find that $\theta(x) = -\pi x/d|_{\text{mod}\pi}$. Next, in order to ensure that no energy is found in the zero-order, we require that $\eta_{\text{E}} = 0$. This condition leads to the solution $t_x = t_y$ and $\phi = \pi$. Thus by determining the incident polarization, $|\mathbf{E}_{\text{in}}\rangle$, the grating orientation, $\theta(x)$, and the grating parameters $t_x = t_y$ and $\phi = \pi$, we are able to create the desired diffraction pattern.

In addition, we note that for such a grating, the DGP for the RPO is $2\theta(x) = -2\pi x/d|_{\text{mod}2\pi}$, and therefore if $|\mathbf{E}_{\text{in}}\rangle = |\mathbf{L}\rangle$, the grating is blazed in the opposite direction. Thus for arbitrary incident polarization, the diffracted energy will be distributed between the 1st and -1st orders. The distribution is dependent on the polarization of the incident beam. Furthermore, the polarization in the first-order will always be $|\mathbf{L}\rangle$, and the polarization in the -1st order will always be $|\mathbf{R}\rangle$. Thus, by switching the incident polarization between an $|\mathbf{L}\rangle$ state and an $|\mathbf{R}\rangle$ state, an optical switch can be realized. Furthermore, if we choose $\phi \neq \pi$, then some of the incident energy will be coupled into the EPO, resulting in the appearance of a zero-order that maintains the polarization of the incident beam, thereby demonstrating the usefulness of such a device as a variable polarization-dependent beam splitter.

We now focus our attention on the design of the blazed grating discussed above using a quasi-periodic subwavelength structure. Since the determination of the grating parameters t_x, t_y and ϕ depend mainly on the subwavelength groove profile, and not on the subwavelength groove orientation, we begin by determining the desired sub wavelength groove orientation, $\theta(x)$, and period, $\Lambda(x,y)$, for the subwavelength structure with the desired DGP. The grating parameters t_x, t_y and ϕ are later determined by choosing a fabrication process that yields a grating profile with the desired birefringence.

To design a continuous subwavelength structure with the desired DGP, we define a subwavelength grating vector, $\mathbf{K}_{\text{g}}(x,y)$, oriented perpendicular to the desired subwavelength grooves

$$\mathbf{K}_g(x,y) = K_0(x,y)\cos(\pi x/d)\hat{\mathbf{x}} - K_0(x,y)\sin(\pi x/d)\hat{\mathbf{y}}. \quad (6)$$

$K_0(x,y) = 2\pi/\Lambda(x,y)$ par is yet to be determined as the local spatial frequency of the subwavelength structure. Fig. 3(c) illustrates this definition of $\mathbf{K}_g(x,y)$. To ensure the continuity of the subwavelength grooves, we require that $\nabla \times \mathbf{K}_g = 0$, leading to the partial differential equation

$$\frac{\partial K_0}{\partial y}\cos(\pi x/d) + \frac{\partial K_0}{\partial x}\sin(\pi x/d) + \frac{\pi}{d}K_0\cos(\pi x/d) = 0 \quad (7)$$

with the boundary condition $K_0(x,0) = 2\pi/\Lambda_0$, where Λ_0 is the local subwavelength period at $y = 0$. The solution to this problem is given by

$$\mathbf{K}_g(x,y) = \frac{2\pi}{\Lambda_0}\exp(-\pi y/d) \times \left[\cos(\pi x/d)\hat{\mathbf{x}} - \sin(\pi x/d)\hat{\mathbf{y}}\right]. \quad (8)$$

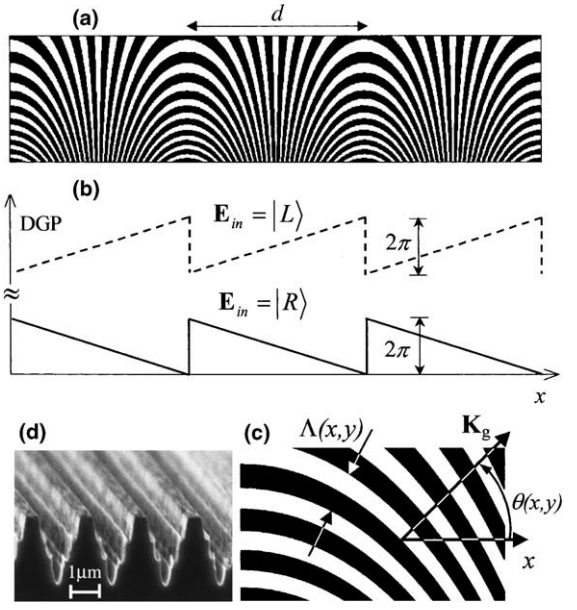

Fig. 3. (a) The magnified geometric representation of the continuous blazed polarization diffraction grating; (b) the resulting DGPs for the RPO and LPO formed by this structure; (c) shows a magnified image of a region on the subwavelength structure, demonstrating the local subwavelength period $\Lambda(x,y)$ the local subwavelength groove orientation $\theta(x,y)$ and the local subwavelength grating vector $\mathbf{K}_g$; (d) scanning electron microscope image of the GaAs dielectric structure.

Consequently, the grating function is then found by integrating $\mathbf{K}_g$ over an arbitrary path to yield

$$\phi_g(x,y) = \frac{2d}{\Lambda_0}\sin(\pi x/d)\exp(-\pi y/d). \quad (9)$$

We realized a Lee-type binary subwavelength structure mask [10] described by the grating function of Eq. (9) using high-resolution laser lithography. The amplitude transmission for such a Lee-type binary mask can be derived as

$$t(x,y) = U_s[\cos(\phi_g) - \cos(\pi q)], \quad (10)$$

where U_s is the unit step function defined by

$$U_s(\eta) = \begin{cases} 1, & \eta \geqslant 0, \\ 0, & \eta < 0 \end{cases}$$

and where q is the duty cycle of the grating which was chosen as 0.5. Fig. 3 illustrates the geometry of a Lee-type binary subwavelength, as well as the resulting DGPs for the RPO and the LPO formed by this structure. The figure shows a continuous quasi-periodic subwavelength structure with a local subwavelength period $\Lambda(x,y)$ where at each location on the element, the grooves are oriented perpendicular to the required fast-axis, resulting in the desired polarization diffraction grating. The resulting DGPs resemble the phase function of a scalar blazed grating. The RPO is blazed in the opposite direction of the LPO as discussed above. Hence, incident $|\mathbf{R}\rangle$ polarization is diffracted in the opposite direction of incident $|\mathbf{L}\rangle$ polarization. The local subwavelength periodicity gives the structure its birefringence, whilst the continuity of the subwavelength grooves ensures the continuity of the resulting field. Furthermore, we note the space-varying nature of $\Lambda(x,y)$. This is a necessary result for the requirement of continuity posed on the subwavelength grooves [5,6].

We realized three different subwavelength structures with the geometry shown in Fig. 3. The first element was realized as a metal stripe subwavelength structure using contact photolithography and lift-off, and the other two elements were dielectric gratings realized using contact photolithography and dry etching techniques. The elements were realized for CO_2 laser radiation at a wavelength of 10.6 on 500 μm thick GaAs wafers. We fabricated the gratings with $\Lambda_0 = 2$ μm, and

$d = 2.5$ mm, consisting of 12 periods of d. The gratings were formed with maximum local subwavelength period of $\Lambda = 3.2$ μm because the Wood anomaly occurs at 3.24 μm for GaAs [5]. The metal stripes consisted of a 10 nm adhesion layer of Ti and 60 nm Au with a duty cycle of 0.6 yielding measured values of $t_x = 0.6$, $t_y = 0.2$, and $\phi = 0.6\pi$. The dielectric gratings were fabricated using electron-cyclotron resonance etching with BCl_3 to nominal depth of 2.5 μm and duty cycle of 0.5, resulting in measured values of a retardation $\phi = \pi/2$, and $t_x = t_y = 0.9$. By combining two such gratings, we obtained a grating with retardation $\phi = \pi$, and $t_x = t_y = 0.89$. These values are close to the theoretical predictions achieved using rigorous coupled wave analysis [11]. Fig. 3(d) shows a scanning electron microscope image of one of the dielectric structures. We note the local periodicity of the structure and the clear profile of the subwavelength grooves.

Following the fabrication we illuminated the structures with polarized light. Fig. 4 shows images of the far-field intensity distributions of the transmitted beams, as well the measured and predicted intensity cross-sections for incident $|\mathbf{R}\rangle$ polarization, for incident $|\mathbf{L}\rangle$ polarization and for incident linear polarization ($|\mathbf{E}_{in}\rangle = |\uparrow\rangle$). There is a good agreement between experiment and theory, which was calculated using Eq. (4), and far-field Fraunhoffer intensities. For incident $|\mathbf{R}\rangle$ polarization only the zero-order and the first-order appear. The zero-order is due to the EPO, and maintains the polarization of the incident beam, whereas the first-order is derived from the LPO and has $|\mathbf{L}\rangle$ polarization. For incident $|\mathbf{L}\rangle$ polarization, the zero-order and the -1st order appear, and the polarization of the -1st order is $|\mathbf{R}\rangle$. In the case of incident linear polarization, we note the linear polarization of the zero-order, the $|\mathbf{L}\rangle$ polarization of the first-order and the $|\mathbf{R}\rangle$ polarization of the -1st as discussed above. We note that for the grating in which $t_x = t_y = 0.89$ and $\phi = \pi$, $\eta_E = 0$, consequently, all of the energy is diffracted into the 1st and -1st orders, as expected.

Fig. 5 shows the predicted and measured diffraction efficiencies for the three blazed polarization diffraction gratings for various incident

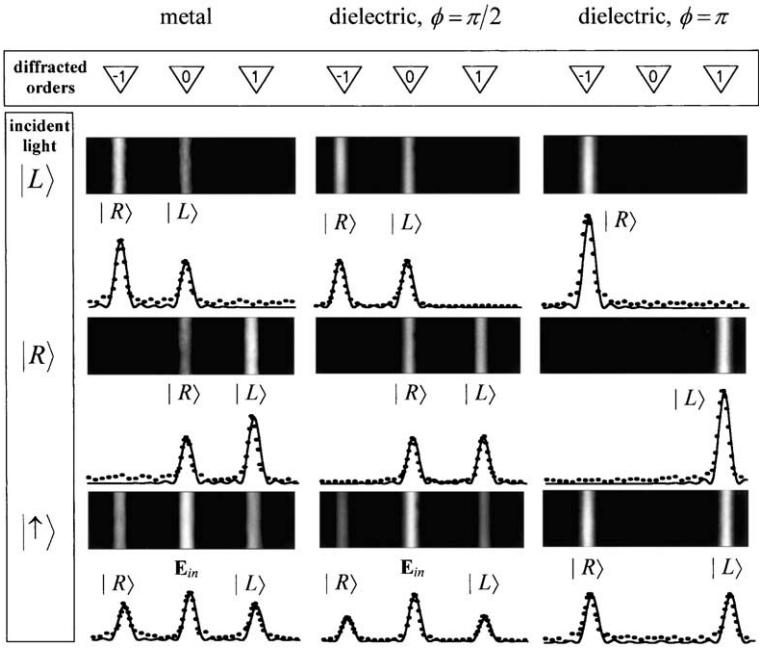

Fig. 4. Images and experimental (dots) and calculated cross-section (solid curves) of the far-field of the beam transmitted through the blazed polarization diffraction gratings, when the incident beam has $|\mathbf{L}\rangle$ polarization, when the incident beam has $|\mathbf{R}\rangle$ polarization, and when the incident beam has linear polarization, $|\uparrow\rangle$.

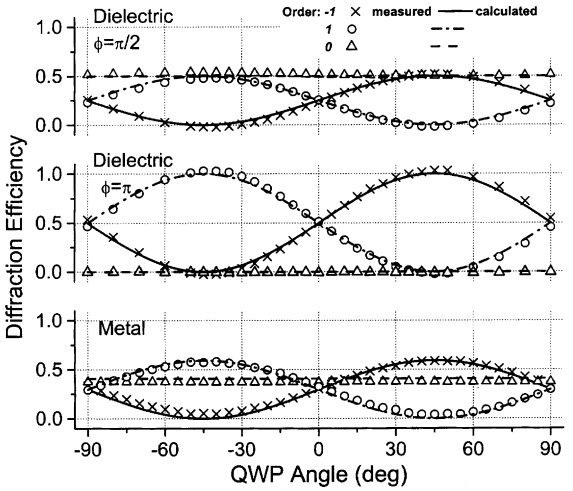

Fig. 5. Measurements and predicted diffraction efficiencies in the 1st, −1st and 0 orders of the metal-stripe and dielectric blazed polarization gratings for various incident polarizations. The different incident polarization were achieved by rotating a quarter waveplate (QWP) in front of the linearly polarized light emitted from the CO_2 laser. The graphs show the efficiencies as a function of the orientation of the QWP. The efficiencies are normalized relative to the total transmitted intensity for each grating.

polarization states. The diffraction efficiencies are normalized relative to the total transmitted intensity. The different polarization-states were achieved by rotating a quarter wave-plate in front of the linearly polarized light emitted from the laser. The experiments agree with the predictions. The diffraction efficiency in the zero-order is equal to η_E. It has a different value for each of the grating, however, for each grating, it remains constant regardless of the incident polarization. On the other hand, the diffraction into the 1st and −1st orders depends on the incident polarization, illustrating the usefulness of polarization diffraction gratings as variable polarization beam-splitters and light modulators.

4. Binary polarization diffraction gratings

To further examine the use of polarization diffraction gratings as beam splitters and optical switches, we fabricated a binary polarization diffraction grating using a subwavelength dielectric structure. Each period, d, ($d > \lambda$), of the grating is

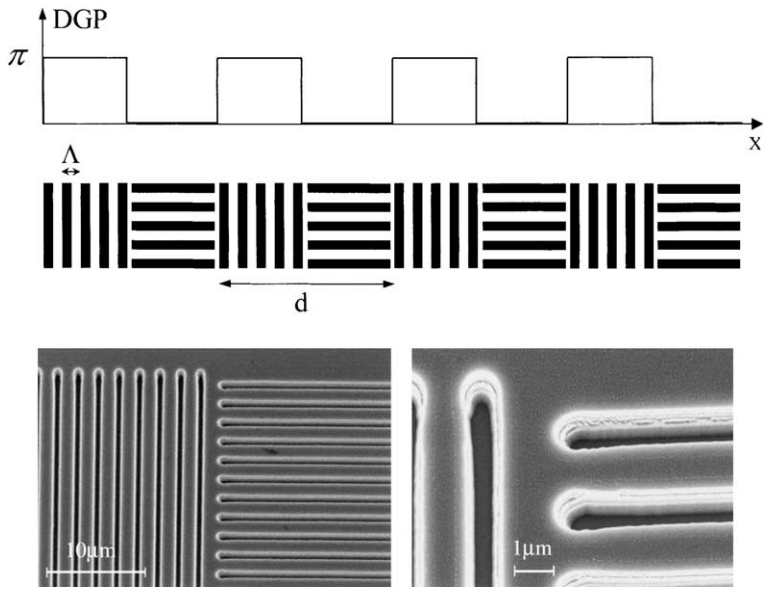

Fig. 6. Geometric representation of the subwavelength structure of the binary polarization diffraction grating (middle), as well as the DGP that results from this structure (top). The pictures at the bottom are scanning electron microscope images of the dielectric subwavelength structure.

comprised of two regions. The subwavelength grating vector in the first region pointed along the x-axis, and the subwavelength grating vector in the second region pointed along the y-axis, i.e.

$$\theta(x) = \begin{cases} 0, & 0 < x < d/2, \\ \pi/2, & d/2 < x < d. \end{cases} \tag{11}$$

We fabricated the subwavelength structure on a GaAs wafer with $t_x = 0.95$, $t_y = 0.84$, and $\phi = 0.45\pi$. The structure was fabricated with $d = 200$ μm and $\Lambda(x,y) = 2$ μm. Fig. 6 shows a schematic representation of the subwavelength structure, a graph depicting the resulting DGP and scanning electron microscope images of the subwavelength structure which we had fabricated. We note that the DGP is the same for both the RPO and the LPO. It resembles a scalar binary π-phase grating. Consequently the diffraction efficiencies for both the RPO and the LPO, will be the same as those of a scalar binary π-phase grating [12] i.e.

$$\eta_m^{\mathrm{R}} = \eta_m^{\mathrm{L}} = \frac{4\sin^2(m\pi/2)}{(m\pi)^2}. \tag{12}$$

Note that for a binary π-phase grating only the odd orders appear and consequently $\eta_0^{\mathrm{L}} = \eta_0^{\mathrm{R}} = 0$. Furthermore, Eq. (12) yields that $\eta_1^{\mathrm{L,R}} = \eta_{-1}^{\mathrm{L,R}} = 0.405$, and $\eta_3^{\mathrm{L,R}} = \eta_{-3}^{\mathrm{L,R}} = 0.045$.

Fig. 7 shows the measured diffraction efficiencies when the incident beam has (Figs. 7(a) and (b)) circular and (Fig. 7(c)) linear polarization, as well as the efficiency when the transmitted beam has passed through a circular polarizer oriented to transmit $|\mathbf{R}\rangle$ polarized light (Figs. 7(d)–(f)). We note that when the beam does not pass through a circular polarizer, the intensity in the various diffracted orders is not dependent upon the incident polarization, however the polarization-state of the diffracted orders does depend on the incident polarization. We note that the intensity of the diffracted orders on the right is equal to the intensity of the diffracted orders on the left, indicative of symmetrical phase structure of the DGP. Furthermore the ratio between the intensity in the first and third orders is $\eta_1/\eta_3 \approx 9$, in agreement with Eq. (12), providing further verification of the binary π-phase of the DGP. In addition, for incident $|\mathbf{R}\rangle$ polarization, the experimental ratio between the intensities in the zero-order and in the first-order is 3.376. This agrees with the predicted ratio of

$$\eta_{\mathrm{E}}/(\eta_{\mathrm{L}}\eta_1^{\mathrm{L}}) = |t_x + t_y e^{i\phi}|^2/(0.405|t_x - t_y e^{\phi}|^2),$$

as predicted using Eqs. (4) and (12).

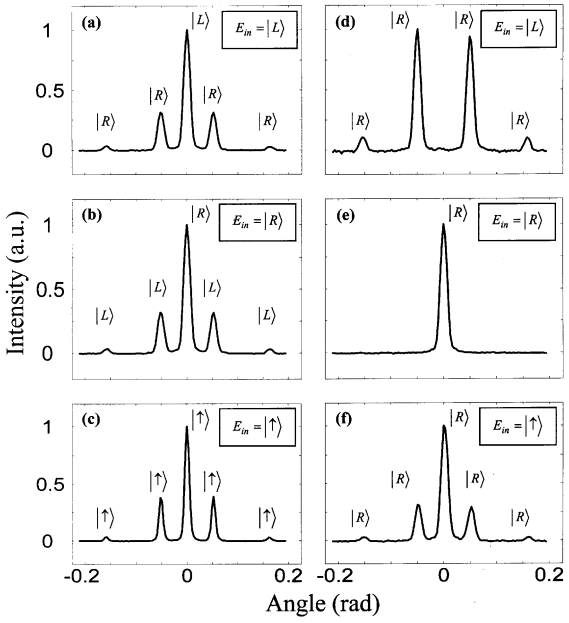

Fig. 7. Measured intensity and polarization in the various diffraction orders of the binary polarization diffraction grating for incident (a) $|\mathbf{L}\rangle$ polarization, (b) incident $|\mathbf{R}\rangle$ polarization and (c) incident $|\uparrow\rangle$ polarization, as well as the intensity transmitted through a combination of the binary diffraction grating and a circular polarizer oriented to transmit $|\mathbf{R}\rangle$ polarization for (d) incident $|\mathbf{L}\rangle$ polarization (e) incident $|\mathbf{R}\rangle$ polarization and (f) incident $|\uparrow\rangle$ polarization. The intensities are normalized so that the maximum intensity in each graph is equal to 1.

When a circular polarizer, oriented to transmit only $|\mathbf{R}\rangle$ polarized light is applied to the beam, we notice that for incident $|\mathbf{R}\rangle$ polarization (Fig. 7(e)) only the zero-order appears (this is because $\eta_{\mathrm{R}} = 0$). For incident $|\mathbf{L}\rangle$ polarization (Fig. 7(d)) only the orders other than the zero-order appear (this is because the EPO has $|\mathbf{L}\rangle$ polarization), and for incident linear polarization (Fig. 7(f)) all diffracted orders appear (this is due all three orders being linearly polarized). Thus, by placing a polarization modulator such as a liquid crystal cell in front of a setup, comprising a polarization–diffraction grating and a circular polarizer, an optical switch could be assembled for appli-

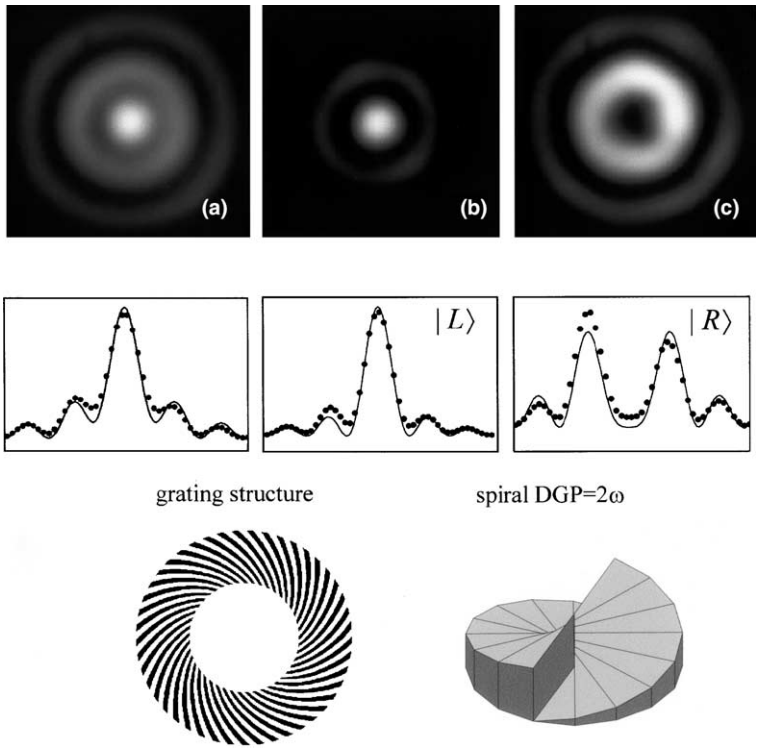

Fig. 8. The far-field images and calculated and measured cross-sections of the beam transmitted through the circular symmetric polarization mode switching: (a) when the incident polarization is $|\mathbf{L}\rangle$ as well as (b) the image and cross-sections of the transmitted $|\mathbf{L}\rangle$ component, and (c) the image and cross-sections of the transmitted $|\mathbf{R}\rangle$ component. Also shown, (bottom), the geometry of the subwavelength quasi-periodic structure as well as the spiral DGP caused by this element.

cations such as optical interconnects in communications.

5. Circular symmetric polarization mode switching

Until now we have discussed polarization beam splitting and optical switching by use of polarization diffraction gratings. However, sometimes a different geometry is required. Suppose for instance, we wish to create an optical switch that enables switching between an optical circularly symmetric mode with a bright center, and an optical circularly symmetric mode with a dark center. This can be done with a quasi-periodic subwavelength structure for which, $\theta(x,y) = \omega(x,y) + c$, where $\omega = \arctan(y/x)$ is the azimuthal angle, and c is a constant number. The DGP of the RPO for such an element is equal to $2(\omega(x,y) + c)$. Thus the RPO carries a vortex with a topological charge of 2 [13], and therefore it has a dark center. Furthermore, since the EPO does not undergo any phase modification, its topological charge is zero, and it exhibits a bright center. Therefore, if we design a quasi-periodic subwavelength structure with $\theta(x,y) = \omega(x,y) + c$, choose $\phi \neq \pi$, and illuminate it with $|\mathbf{L}\rangle$ polarization, the resulting beam will comprise an $|\mathbf{R}\rangle$ polarized vortex carrying beam with a dark center and an $|\mathbf{L}\rangle$ polarized beam with a bright center. We can switch between the two modes using a circular polarizer.

We realized such a quasi-periodic subwavelength structure on a GaAs wafer, with $\theta(x,y) = \omega(x,y) + \pi/4$, yielding a grating function $\phi_g = [2\pi r_0/(\sqrt{2}\Lambda_0)][\ln(r/r_0) - \omega]$, where r is a radial coordinate. We chose $\Lambda_0 = 2$ μm and $r_0 = 5$ mm, so that $5\text{ mm} < r < 8\text{ mm}$ and $2\ \mu\text{m} < \Lambda < 3.2\ \mu\text{m}$, and fabricated a dielectric grating with

retardation of $\phi = \pi/2$. Note that for incident $|\mathbf{L}\rangle$ polarization, the transmitted beam had radial polarization in the near field, and that for incident $|\mathbf{R}\rangle$ polarization, the near field had azimuthal polarization. Fig. 8 shows far-field images and the measured and calculated cross-sections of (a) the transmitted beam when the incident polarization is $|\mathbf{L}\rangle$ as well as the far-field image of the (b) $|\mathbf{L}\rangle$ and (c) $|\mathbf{R}\rangle$ components of the beam as obtained with a circular polarizer. Fig. 8 also shows the geometry of the subwavelength quasi-periodic structure as well as the DGP caused by this element. We note the clear vortex in the DGP. The dark center of the vortex is evident in the measured results where we note that the $|\mathbf{L}\rangle$ component of the transmitted beam (the EPO), has a bright center without undergoing any phase modification, whereas the $|\mathbf{R}\rangle$ component (RPO) has a dark center, clearly indicative of its topological charge. The results clearly demonstrate the circularly symmetric mode switching, which can be realized using subwavelength periodic structures.

6. Conclusions

To conclude, we have demonstrated polarization diffraction gratings as polarization-sensitive beam-splitters, as well as optical switches. We have demonstrated that the application of subwavelength quasi-periodic structures, for this purpose, is not limited to optical switches based on linear polarization diffraction gratings, and that more complex designs are possible. The introduction of space-varying geometrical phases through space-variant polarization manipulations, enables new approaches for beam-splitting and the fabrication of novel polarization-sensitive optical elements.

References

[1] J.A. Davis, J. Adachi, C.R. Fernández-Pousa, I. Moreno, Opt. Lett. 26 (2001) 587.
[2] F. Gori, Opt. Lett. 24 (1999) 584.
[3] J. Tervo, J. Turunen, Opt. Lett. 25 (2000) 785.
[4] B. Wen, R.G. Petschek, C. Rosenblatt, Appl. Opt. 41 (2002) 1246.
[5] Z. Bomzon, V. Kleiner, E. Hasman, Opt. Commun. 192 (2001) 169.
[6] Z. Bomzon, V. Kleiner, E. Hasman, Opt. Lett. 26 (2001) 33.
[7] Z. Bomzon, G. Biener, V. Kleiner, E. Hasman, Opt. Lett. 27 (2002) 285.
[8] Z. Bomzon, V. Kleiner, E. Hasman, Opt. Lett. 26 (2001) 1424–1426.
[9] Z. Bomzon, G. Biener, V. Kleiner, E. Hasman, Opt. Lett. 27 (2002) 1141.
[10] W.H. Lee, Appl. Opt. 13 (1974) 1677.
[11] M.G. Moharam, T.K. Gaylord, J. Opt. Soc. Am. A 3 (1986) 1780.
[12] E. Hasman, N. Davidson, A.A. Friesem, Opt. Lett. 16 (1991) 423.
[13] D. Rozas, C.T. Law, G.A. Swartzlander Jr., J. Opt. Soc. Am. B 14 (1997) 3054.